



Hydrodynamic Simulations of a FOWT Platform (1st FOWT Comparative Study) Using OpenFOAM Coupled to MoodyCore

Eskilsson, Claes; Verao Fernandez, Gael; Andersen, Jacob; Palm, Johannes

Published in:

The Proceedings of the 33rd (2023) International Ocean and Polar Engineering Conference

Publication date:
2023

Document Version
Early version, also known as pre-print

[Link to publication from Aalborg University](#)

Citation for published version (APA):

Eskilsson, C., Verao Fernandez, G., Andersen, J., & Palm, J. (2023). Hydrodynamic Simulations of a FOWT Platform (1st FOWT Comparative Study) Using OpenFOAM Coupled to MoodyCore. In *The Proceedings of the 33rd (2023) International Ocean and Polar Engineering Conference* (pp. 461-468). International Society of Offshore & Polar Engineers.

General rights

Copyright and moral rights for the publications made accessible in the public portal are retained by the authors and/or other copyright owners and it is a condition of accessing publications that users recognise and abide by the legal requirements associated with these rights.

- Users may download and print one copy of any publication from the public portal for the purpose of private study or research.
- You may not further distribute the material or use it for any profit-making activity or commercial gain
- You may freely distribute the URL identifying the publication in the public portal -

Take down policy

If you believe that this document breaches copyright please contact us at vbn@aub.aau.dk providing details, and we will remove access to the work immediately and investigate your claim.

Hydrodynamic Simulations of a FOWT Platform (1st FOWT Comparative Study) Using OpenFOAM Coupled to MoodyCore

Claes Eskilsson^{1,2}, Gael Verao Fernandez², Jacob Andersen², Johannes Palm³

¹RISE - Research Institutes of Sweden, Borås, Sweden

²Department of the Built Environment, Aalborg University, Aalborg, Denmark

³Sigma Energy & Marine AB, Gothenburg, Sweden

ABSTRACT

We numerically simulate the hydrodynamic response of a floating offshore wind turbine (FOWT) using CFD. The FOWT under consideration is a slack-moored 1:70 scale model of the UMaine VoltumUS-S semi-submersible platform. This set-up has been experimentally tested in the COAST Laboratory Ocean Basin at the University of Plymouth, UK. The test cases under consideration are (i) static equilibrium load cases, (ii) free decay tests and (iii) two focused wave cases with different wave steepness. The FOWT is modelled using a two-phase Navier-Stokes solver inside the OpenFOAM-v2006 framework. The catenary mooring is computed by dynamically solving the equations of motion for an elastic cable using the MoodyCore solver. The results of the static and decay tests are compared to the experimental values with only minor differences in motions and mooring forces. The focused wave cases are also shown to be in good agreement with measurements. The use of a one-way fluid-mooring coupling results in slightly higher mooring forces, but does not influence the motion response of the FOWT significantly.

KEY WORDS: Floating offshore wind turbine; mooring; computational fluid dynamics.

INTRODUCTION

Offshore wind is a rapidly expanding industry. In 2019, 146 offshore wind farms with a total of 27.2 GW installed power were in operation globally (WFO 2020). Specifically, floating offshore wind turbines (FOWTs) have entered the commercialization phase. Outside Scotland the 30 MW Hywind farm has been in operation since 2017 using a spar-type design. The 27MW Windfloat Atlantic was commissioned in 2020 18 km of the Portuguese coast, and the 50MW Kincardine floating offshore wind farm became operational in 2021 in Scottish waters. Both of the latter projects use Principle Power's Windfloat semi-submersible. Still, many new concepts of FOWT are under development, and, in addition, the ever growing turbine size is putting new demands on the floaters.

Numerical modelling of FOWT are typically done with aero-elasto-control-hydro-mooring software, e.g., OpenFAST (OpenFast 2023) and DeepLines Wind (Principia 2023). Focusing on the hydrodynamic modelling these models are based on standard linear potential flow (LPF) assumptions and approximations. The mooring modelling is usually of dynamic type using lumped masses or finite element methods. Models based on LPF are computationally efficient but loose accuracy for survival cases with highly nonlinear waves. Additionally, within the OC5 projects problems relating to low-frequency response were identified when using LPF models, see Wang et al. (2021). High-fidelity models overcome the above problems, but the computational cost is quite high.

Blade resolved high-fidelity modelling of FOWTs have been presented by, e.g., Liu et al. (2017) and Zhou et al. (2022). These are very complete simulations but with a very high computational cost. Often the aerodynamic part is simplified using actuator disc or lines approaches, e.g., Cheng et al. (2019) and Yu et al. (2023).

Focusing specifically on the hydrodynamic part of the floater, Burmester et al. (2020) performed extensive verification and validation (V&V). Also Wang et al. (2021) looked into V&V of the hydrodynamic performance of FOWT. As expected, they found that mesh resolution is the limiting factor for the numerical uncertainty. Looking at the hydro-mooring coupling, Burmester et al. (2020) showed that the inertia and drag of the mooring lines could have an influence on the uncertainty of the overall motion response. Typically, the inertia and drag are found from either quiescent fluid or from a linear super-positioning of regular waves. With regard to the mooring a one-way coupling – to use the fluid velocities sampled in the CFD domain at the mooring nodes and used to compute added mass and drag forces acting on the cables – have been developed in a few studies (de Lataillade 2019, Martin & Bihs 2021, Eskilsson & Palm 2022).

In this paper we model the motion response, due to hydrodynamic loading only, of a slack-moored FOWT using CFD and dynamic mooring. In Eskilsson and Palm (2022) the DeepCwind semi-submersible

(Robertson et al. 2017) was modelled using a one-way fluid-mooring coupling. Virtually no influence of using the real fluid velocity compared to a quiescent fluid was seen in the mooring loads. However, the case investigated in Eskilsson and Palm (2022) was a mild regular wave. In the present work we investigate the effect of including fluid-mooring coupling for a harsh survival condition simulation, realised by focused waves.

NUMERICAL MODELS

Reynolds-Averaged Navier-Stokes equations

We solve the wave-structure interaction problem using the Reynolds Averaged Navier-Stokes equations with air-water interface capturing using the volume of fluid method (VOF-RANS). The numerical model used is the `interFoam` model, which is part of the widely used open-source framework `OpenFOAM` (OpenFOAM 2020, Weller et al. 1998). The 2006 version is employed in this study. `OpenFOAM` is based on a cell-centred 2nd order finite volume method on unstructured polyhedral cells. The standard $k-\omega$ -SST model (Menter et al. 2003) is used throughout this paper as turbulence model, together with a continuous wall function approach.

Wave generation/absorption is in the present work carried out by means of relaxation zones (Jacobsen et al. 2012).

Mooring

The VOF-RANS model is coupled to a dynamic mooring solver – `moodyCore` (Palm et al. 2017, Palm and Eskilsson 2018). `moodyCore` solves the elastic cable equation – including bending but disregarding torsion – using a high-order discontinuous Galerkin method. `moodyCore` can be coupled to `interFoam` using a quadratic interpolation to account for the difference in time steps size between the CFD and mooring solver (Palm et al. 2016). The cable fairleads are attached to the FOWT using the `externalPoint` boundary condition – meaning that the 3DoF positions of the attachment points are directly transferred from the CFD model to the mooring solver and that `moodyCore` returns the forces in global coordinate system at the attachment points. The `moodyCore` library and the mooring restraint as implemented in `OpenFOAM` can be downloaded from github.com/johannep/moodyAPI.

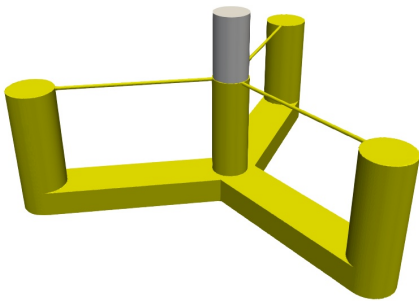


Fig. 1 3D view of the FOWT.

FOWT CASE

The FOWT under consideration is a slack-moored 1:70 scale model of the UMaine VoltturnUS-S semi-submersible platform (Allen et al. 2020). The FOWT is made up of three outer cylinders (diameter 0.1778 m and height 0.5 m) and a central cylinder (diameter 0.143 m and height 0.5 m). The outer cylinders are equiangularly spaced in a distance of 0.7393 m to the center of the central cylinder. The outer and central cylinders are connected by pontoons (width 0.1778 m and height 0.100 m) at the bottom of the cylinders, as well as with braces (diameter 0.013 m) at the top of the cylinders. A tower (diameter 0.13592 m and height 1.851 m) is mounted atop the central column. Attached to the tower is a simplified nacelle-rotor with a hub height of 2.476 m from the bottom of the cylinders. See Fig. 1.

The FOWT has been experimentally tested in the COAST Laboratory Ocean Basin at the University of Plymouth, UK (Ransley et al. 2022). All experimental data used in this work are found in Ransley et al. (2022). We define the origin of the global coordinate system to be located at the still water level free surface at the middle of the central

Table 1 Environmental parameters. * denotes that the coefficient is given as ratio of critical damping.

Water density	998.2 kg/m ³
Ground stiffness	3.0E05 Pa/m
Ground damping coefficient*	1.0
Ground friction coefficient	0.3

Table 2 Properties of the FOWT (in body coordinate system with origin at the bottom of and in the middle of the centre column).

Mass	56.3 kg
Moments of inertia (I _{xx} , I _{yy} , I _{zz})	(26.68, 26.68, 14.18) kg m ²
Center of mass (CoM)	(-0.00477, 0.0, 0.26369) m
Fairlead position - fore	(-0.8392, 0.0, 0.08571) m
Fairlead position - aft-port	(0.4196, -0.7268, 0.08571) m
Fairlead position - aft-starboard	(0.4196, 0.7268, 0.08571) m
Offset to unmoored equilibrium pos.	(0, 0, -0.26495) m
Rotation around unmoored CoM	(0.0, -1,728 0.0)°
Offset to moored equilibrium pos.	(-0.01561, 0, -0.28755) m
Rotation around moored CoM	(0.0, -1,502 0.0)°

Table 3 Properties of the mooring system (assuming a global coordinate system with origin at the free surface in the centre column). * denotes values based on the nominal diameter.

Dry mass per meter	0.144 kg/m
Axial stiffness	1.0E04 kgNs
Density	7850 kg/m ³
Drag coefficient*	1.5
Added mass coefficient*	1.0
Anchor position - fore line	(-9.525, 0, -2.86) m
Cable length - fore line	9.685 m
Anchor position - aft-port line	(4.412, -7.655, -2.86) m
Cable length - aft-port	9.017 m
Anchor position - aft-starboard line	(4.412, 7.655, -2.86) m
Cable length - aft-starboard line	9.017 m

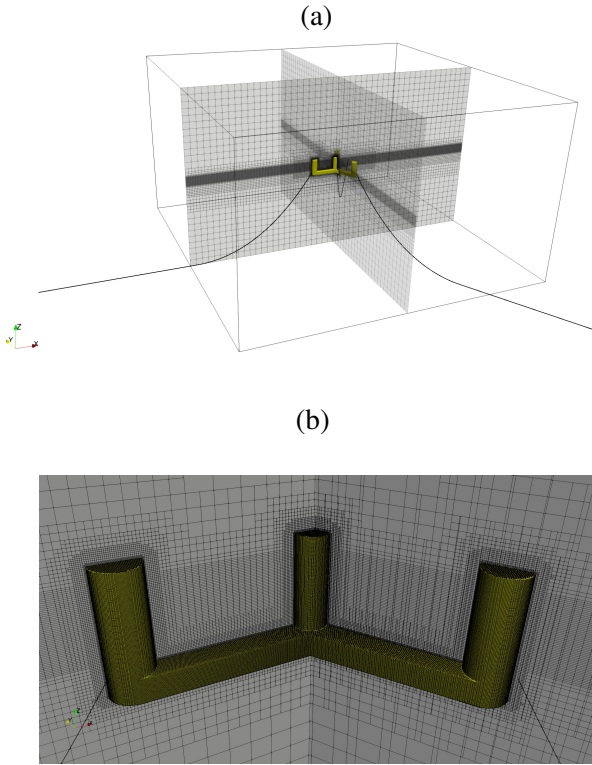


Fig. 2 CFD mesh for the decay cases. (a) global mesh layout, and (b) zoom in on the FOWT structure.

column of the FOWT. The physical wave basin has the dimensions $x \in [-17.3, 17.7]$ m and $y \in [-7.75, 7.75]$ m with a still water depth of 2.86 m. The wave paddles are located at $x = -17.3$ m and there is an absorbing beach starting downstream of the FOWT at $x = 4.5$ m.

The specific parameters for the case are presented in Tables 1–3. Please note that (i) the stiffness and hydrodynamic coefficients for the mooring chain have not been experimentally determined but are taken as standard values (DNV 2010), and (ii) the fore and aft mooring lines were not of equal length in the experiments due to the constraints of the wave basin side walls.

NUMERICAL SET-UP

The computational mesh is created using the `snappyHexMesh` utility in `OpenFOAM`, which creates oct-tree hexahedral dominated meshes from STL surfaces of the body. For the decay tests the computational domain is $x \in [-5, 5]$, $y \in [-5, 5]$, $z \in [-2.86, 2.86]$ m, with 1 m wide sponge zones applied along the outer boundaries. The computational mesh is a full 3D domain made up from 4.2M cells, see Fig. 2. There are refinement zones at the free surface as well as around the FOWT. We disregard the bracing and the tower in the simulations, but keep their inertial contributions. The maximum y^+ values for the FOWT are less than 300 throughout all simulations. For the focused wave cases the computational domain is $x \in [-15, 15]$, $y \in [-5, 5]$, $z \in [-2.86, 2.86]$ m, with 10 m wide sponge zones applied at the upstream and downstream boundaries, yielding a cell count of 27.4M. The mesh resolution is based on 20 cells per wave height and 200 cells per wavelength (based on an equivalent regular wave for the focused wave cases).

All outer side boundaries are treated as walls with slip condition applied. Also the bottom boundary is treated as a slip wall. The upper atmospheric boundary is set to a zero total pressure condition. The numerical schemes used in `interFoam` are second-order van Leer scheme for convection terms, second-order central differences for diffusion terms, while the turbulence equations are solved using the first-order upwind method. The time-stepping is carried out using the first-order backward Euler scheme with a CFL number of 0.5.

The mesh morphing algorithm used for the moving mesh employs a spherical linear interpolation (SLERP) approach (Shoemake 1985). In the present work we use the modified mesh morphing algorithm presented in Palm and Eskilsson (2022). The modified approach decouples the rotational and translation degrees of freedom of the mesh morphing, yielding a more stable mesh morphing for large motions.

The mooring cables are discretized into 20 finite elements of 5:th order and `moodyCore` uses an explicit 3:rd order Runge-Kutta scheme with a CFL number of 0.5 to integrate in time. We did an initial test also with 10 elements for the decay tests presented below, with no visible difference between the simulations. Indeed, with 20 elements we expect a somewhat over-resolved mooring solution, since as a rule of thumb 10 5:th order elements give good results for catenary mooring when no snap loads occur. As seen in Fig. 2, the mooring lines extends outside the CFD domain. Please note that the hydrodynamic loads applied to the mooring lines outside the CFD domain assume quiescent flow.

RESULTS AND DISCUSSION

Mooring forces using measured positions

We start by examining the tensions in the cables of the mooring system defined above by running `moodyCore` as a stand-alone mooring solver. The time-series of the fairlead positions are obtained from the measured CoM and rotations using the `externalRigidBody` boundary condition in `moodyCore` (Palm & Eskilsson 2018). This exercise gives baseline results, helping out to judge the mooring results obtained later, as the mooring system definition is somewhat uncertain. However, please note that we have not used this exercise to alter the mooring system to provide a better fit to the experimental data.

Static case. Running the mooring solver with fixed fairlead positions, using a CoM of $(-0.0204, 0, -0.0239)$ m and a pitch angle of -1.502° , the simulated tensions are 7.22 and 7.39 N in the fore cable and aft cables, respectively. This differs from the recorded tensions of 7.6 and 7.2 N. It is a bit concerning that we get lower tension in the fore line compared to the aft lines, while the measurements show the reverse. Nevertheless, the tensions are in the same order of magnitude. Considering the difficulty in getting accuracy tension readings for scaled devices, and the incomplete data for the mooring system, we are content with this result.

Decay cases. The simulated and experimental mooring tensions for the surge, heave and pitch decay tests are presented in Fig. 3. Generally, the comparisons are favorable. The tension in the fore cable is under-estimated throughout the simulations, the offset originates from the initial tension. There is a good fit for the aft lines.

Focused wave cases. Figure 4 shows the comparison between numerical experimental tensions for the two focused wave cases. As for the decay cases we see that the fore cable tensions capture the dynamics but have an offset throughout the simulations. The aft lines have a smaller tension

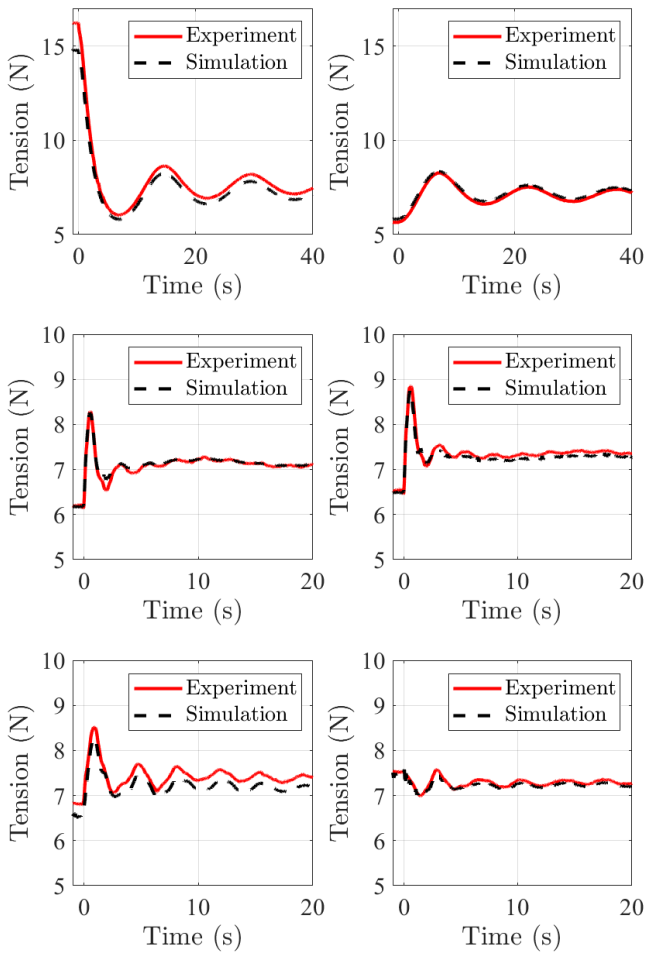


Fig. 3 Tension history for the decay tests using measured CoM. Left column: fore line, and right column: aft lines. Top row: surge decay test, middle row: heave decay test, and bottom row: pitch decay test.

amplitudes and a good fit.

Static equilibrium tests

In order to more rapidly achieve the static equilibrium positions we added damping terms in both the translation and rotational DoF (using damping coefficients of 10 Nm/s and 10 Nms/rad, respectively).

Unmoored case. We start the simulation from the given CoM of (0.0048, 0, -0.0013) m and a pitch angle of -1.728° . After 60 s of simulation time the FOWT is settled on an equilibrium position given by a CoM of (0.0051, 0.0000, 0.0019) m and a pitch angle of -1.464° . The surge position is of course arbitrary and due to initial transients of the surge-pitch coupling. The differences in heave (+0.0031 m) and pitch (0.264°) are deemed small and acceptable.

Moored case. Running moodyCore as a stand-alone mooring solver with the provided static fairlead positions in the previous section, we saw that we got a resulting mooring force of 1.2 N in the surge direction. We thus expect the FOWT to surge a bit until it finds equilibrium, but we nevertheless start from the provided data: CoM at (-0.0204, 0, -0.0239) m and a pitch angle of -1.502° . After 60 s of simulation time the FOWT is settled on an equilibrium position given by

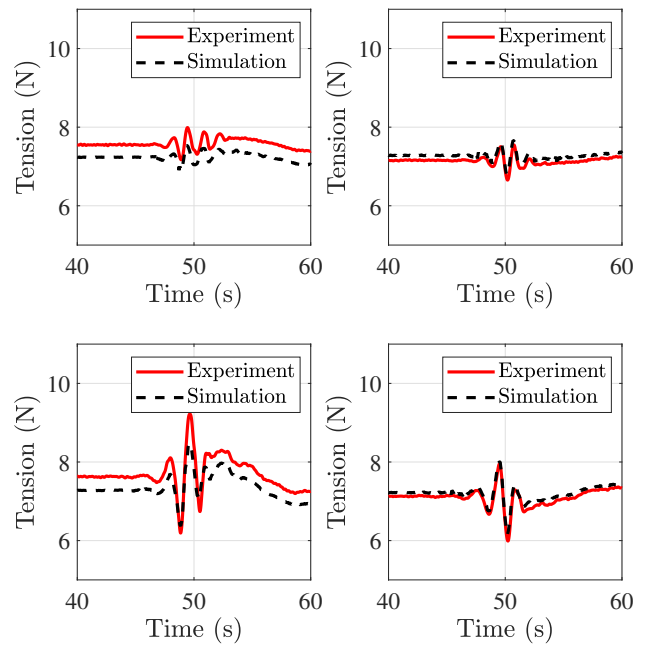


Fig. 4 Tension history for the focused wave tests using measured CoM. Left column: fore line, and right column: aft lines. Top row: benign wave case, and bottom row: harsh wave case.

a CoM of (-0.0128, 0.0000, -0.0188) m and a pitch angle of -1.341° . The differences to the experimental values are: +0.0076 m in surge, +0.0051 m in heave, and $+0.161^\circ$ in pitch.

The resulting tension forces are found to be 7.30N for the fore cable and 7.34N for the aft cables. This, again, differs from the measured data, but is smaller than the difference from the fixed fairleads case. The smaller difference is in line with a smaller pitch angle. In all we judge the results to be within the experimental uncertainty.

Moored decay tests

For the decay tests we use the equilibrium position from the previous section as starting position and then apply the offsets for surge, heave and pitch as given in Table 4. Please note that the figures presented below show results from the offsets applied to the equilibrium position recorded in the moored static equilibrium case. Minor discrepancies to the experimental values are thus to be expected.

Surge decay. Figure 5 show the computed surge, heave and pitch motions as well as the tensions in the mooring cables compared to measurements for the surge decay test. Generally, the fit is good. The most notable difference is that the surge amplitude is slightly over-predicted in the simulation compared to the experiment. The offset in heave is as expected from the static condition test. The initial tension

Table 4 Decay tests offset.

Case	Offset in surge	Offset in heave	Offset in pitch
Surge decay	0.3517m	-0.0012m	-0.7662°
Heave decay	-0.0149m	-0.1473m	0.471°
Pitch decay	-0.0031m	-0.0269m	-9.7508°

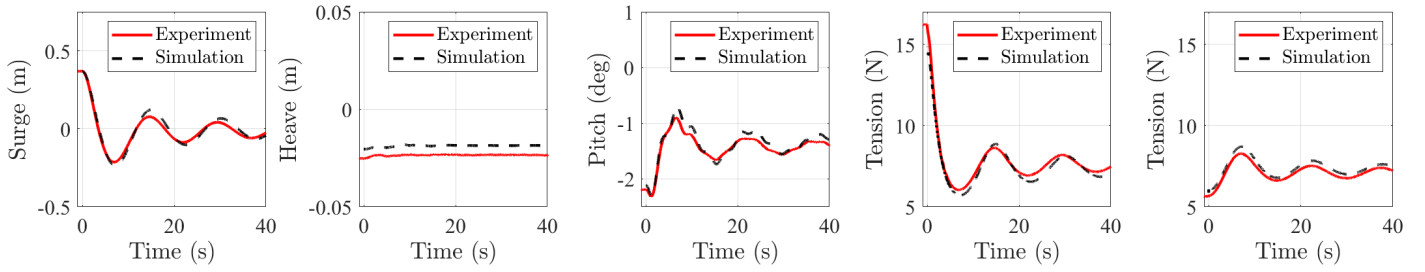


Fig. 5 Surge decay test. From left to right the sub-figures show: surge, heave, pitch, tension fore cable and tension aft cables.

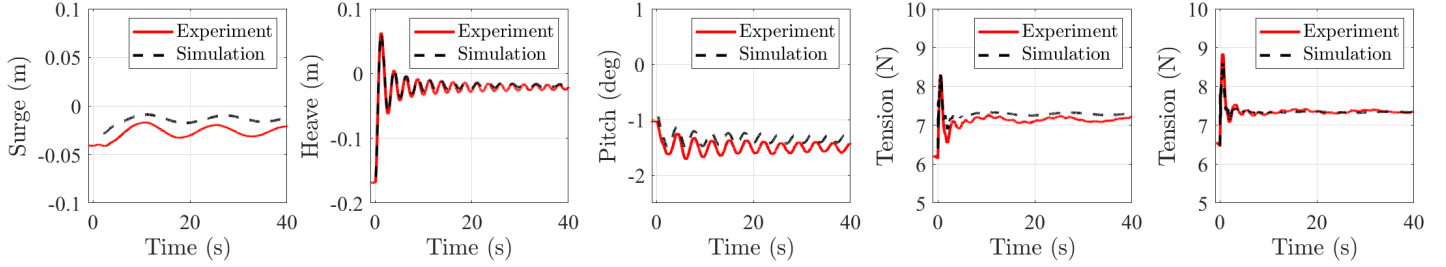


Fig. 6 Heave decay test. From left to right the sub-figures show: surge, heave, pitch, tension fore cable and tension aft cables.

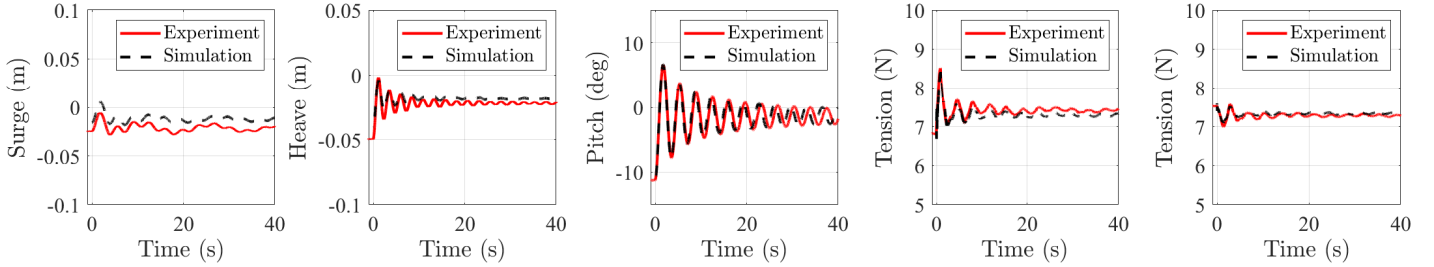


Fig. 7 Pitch decay test. From left to right the sub-figures show: surge, heave, pitch, tension fore cable and tension aft cables.

in the fore cable is slightly under-predicted by the simulation, and subsequently slightly over-predicted for the aft lines.

Heave decay. The simulated surge, heave and pitch motions as well as the tensions in the mooring cables compared to measurements for the surge decay test are presented in Fig. 6. The heave response is very well captured in both amplitude and phase. There is a positive offset in the surge response, causing a slightly larger tension in the fore line.

Pitch decay. Computed and measured surge, heave and pitch motions and mooring line tensions for the pitch decay test are illustrated in Fig. 7. While the simulated pitch amplitude is excellent the pitch period is slightly too small. There are minor positive offsets for the surge and heave response, as expected from the static equilibrium test.

The numerical and experimental data of the decay tests are summarized in Table 5 in terms of decay periods and exponential decay constants. We present only the main mode of motion for each case, e.g. for the surge decay test we present the surge decay period and surge decay constant. The values are computed using the first five oscillations. The decay periods are quite accurately computed, the error ranges between 0.8 to 2.5%. The decay constants show slightly larger errors, in the range of 0.7 to 7.2% error, where it is heave that exhibits the largest error. Please note that all restoring stiffness in surge is due to the mooring system. The ex-

cellent match in surge natural frequency therefore demonstrates that the mooring-coupling does provide accurate low-frequency mooring forces to the FOWT.

Focused wave tests

Two focused wave cases are simulated, one benign state and one harsh state. The focused waves are generated using linear dispersive focusing described by the NewWave theory (Tromans et al. 1991) based on a Pierson-Moskowitz spectrum. The crest amplitude is estimated as $A_{cr} = \sqrt{2H_{m0} \ln(1000)}$, where H_{m0} is the significant wave height. The focus location is $x = 0$ m (in global coordinates) and the focus time is

Table 5 Decay periods and exponential decay constants for the different decay tests.

Case	Mode	Period (s)	Constant (-)
Exp. surge	surge	14.92	7.91E-02
Num. surge	surge	15.28	7.85E-02
Exp. heave	heave	2.50	0.56
Num. heave	heave	2.52	0.52
Exp. pitch	pitch	3.59	2.13E-01
Num. pitch	pitch	3.50	2.14E-01

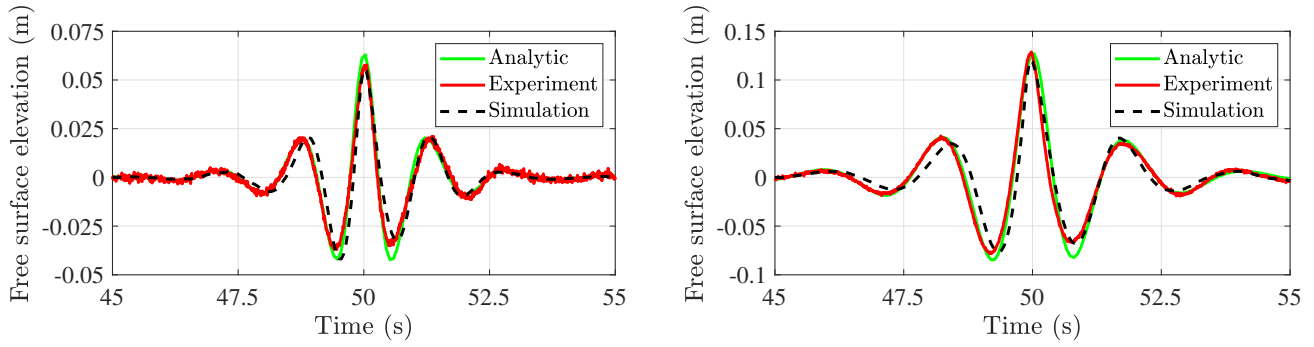


Fig. 8 Free surface elevation at WG6 ($x = 0m$). Left: benign case, and right: harsh case.

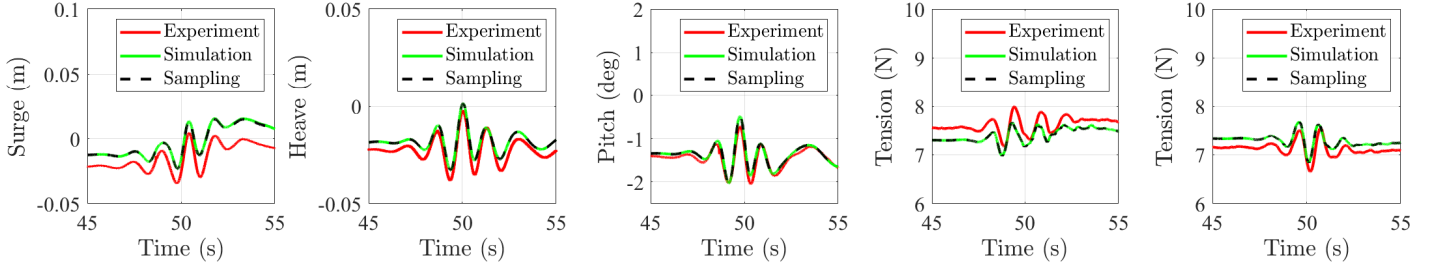


Fig. 9 Benign focused wave test. From left to right the sub-figures show: surge, heave, pitch, tension fore cable and tension aft cables. 'Sampling' denotes simulation using the one-way fluid-mooring coupling.

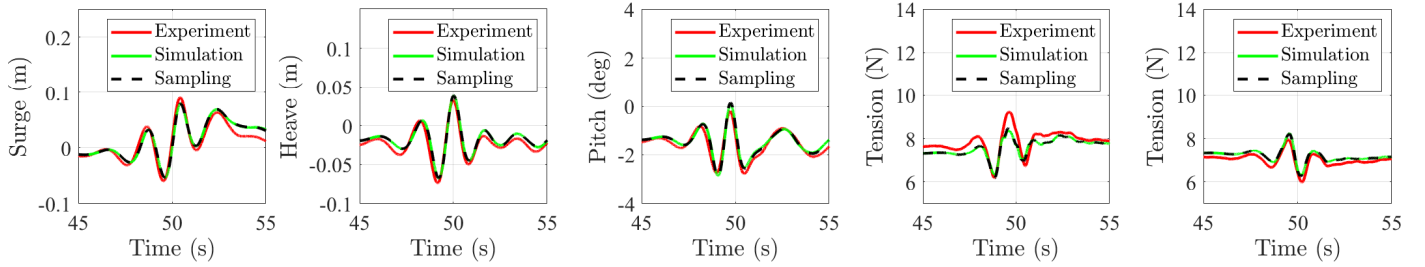


Fig. 10 Harsh focused wave test. From left to right the sub-figures show: surge, heave, pitch, tension fore cable and tension aft cables. 'Sampling' denotes simulation using the one-way fluid-mooring coupling.

$t = 50s$. The wave parameters for the two cases are presented in Table 6. As the experimental tests employed 112 equidistant wave components in the frequency range $f \in [0.15, 2]Hz$, we used the `waves2Foam` utility (Jacobsen et al. 2012) to generate 112 equidistant wave components in the same range for the numerical simulations.

The focused wave cases were each simulated using 8 compute nodes at the Tetralith HPC cluster at the National Supercomputer Centre, Linköping University, Sweden. Each compute node consists of two Intel Xeon Gold 6130 CPUs with 16 CPU cores each, giving that the focused wave simulations were run using 256 cores.

Wave propagation. We first compare the simulated free surface elevation for empty tank tests. In the simulations we use a shorter wave basin and we thus only look at the surface elevation recorded at the centred wave gauge (WG6) located at $x = 0m$. Figure 8 shows the recorded experimental and numerical free surface elevation, as well as the analytical elevation obtained by linear superposition. We see that for both cases the peaks are fairly well predicted both in amplitude and phase. The simulated troughs preceding the peak are lagging in time,

while the following troughs have a better fit with the experimental data. Comparing to the experiments the linear expression predicts a symmetric distribution around the peaks, while both the experimental and numerical records show a deeper preceding trough and a shallower following trough. The difference between the measured and simulated wave elevation is due to a slightly too low resolution in the x -direction, but in order to keep down the cell count we do not further refine the mesh.

Benign case. Figure 9 shows the results for the benign wave case. We see that there is virtually no difference in the simulated results when

Table 6 NewWave parameters using the Pierson- Moskowitz wave spectrum.

Parameter	Benign case	Harsh case
Peak period (T_p)	1.3831s	1.9380s
Significant wave height (H_{m0})	0.069m	0.139m
Crest elevation (A_{cr})	0.064m	0.127m

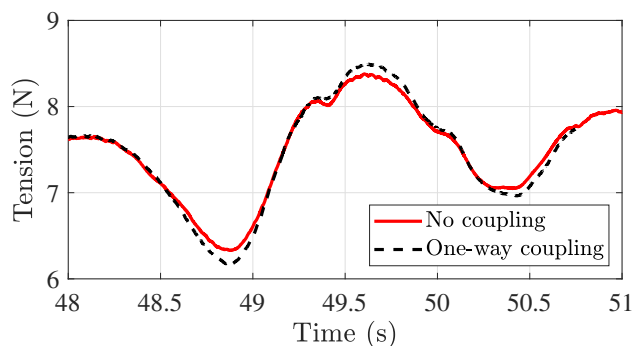


Fig. 11 Tension at the fairlead in the fore cable for the harsh focused wave case.

using the one-way coupling. This is in line with previous experience for cases of rather linear nature. From Fig. 9 we see that the dynamics of the response of the FOWT is in general well captured. The major differences are again the offsets in surge and heave, as well as in the tension.

Harsh case. Like in the benign case the harsh wave case does not show a clear influence of using the one-way coupling, see Fig. 10. However, looking closer on the mooring cables, see Fig. 11, we see that the tension in the fore cable is clearly larger when the coupling is used. However, this difference is not carried over to the motion response. The most obvious difference is that the maximum recorded pitch angle increases with 0.1° , from 0.05° to 0.15° . It is believed that the influence on the response of using the one-way coupling would be more pronounced for an embedded focused wave.

The simulated responses shown in Fig. 10 have good fit to the measured data. Please note that the offsets in surge and heave are similar to the benign case, but are cloaked by the larger responses. The simulated tensions look a lot like the results using the measured fairlead positions (see Fig. 4).

Table 7 shows a comparison of the motion responses between the experiments and simulations in terms of maximum and minimum motions during the impact of the focused waves, i.e. $t \in [48, 52]$ s. We focus on the motion range, simply defined as (max – min), as we then remove the influence of any initial offsets. The largest errors are found

Table 7 Recorded extreme motions for the focused wave cases when $t \in [48, 52]$ s.

Case	Mode	Max	Min	Max-Min
Exp. benign	surge (m)	4.37E-03	-34.45E-03	38.83E-03
Num. benign	surge (m)	15.40E-03	-22.98E-03	38.38E-03
Exp. benign	heave (m)	-2.10E-03	-38.40E-03	36.30E-03
Num. benign	heave (m)	1.35E-03	-32.77E-03	34.13E-03
Exp. benign	pitch ($^\circ$)	-0.72	-2.05	1.33
Num. benign	pitch ($^\circ$)	-0.49	-2.03	1.54
Exp. harsh	surge (m)	90.31E-03	-59.43E-03	149.74E-03
Num. harsh	surge (m)	79.11E-03	-53.56E-03	132.67E-03
Exp. harsh	heave (m)	32.70E-03	-73E-03	106.42E-03
Num. harsh	heave (m)	38.45E-03	-67.47E-03	105.92E-03
Exp. harsh	pitch ($^\circ$)	-0.21	-2.78	2.56
Num. harsh	pitch ($^\circ$)	0.64	-2.86	2.92

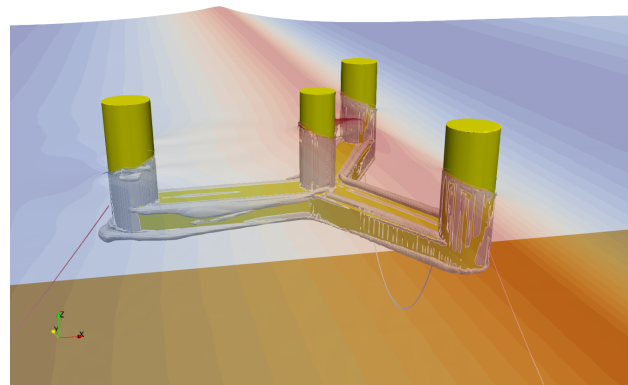


Fig. 12 Snapshot of the FOWT at $t = 50$ s for the harsh focused wave case. The contour show the $Q = 10$ iso-surface.

in the pitch response with 15.5 and 14.1% error for the benign and harsh cases, respectively. The surge response in the harsh wave show a 11.4% error, to be compared to only 1.1% for the benign case, even though the benign case has a larger offset error. The heave response show the smallest error: 5.8% error for the benign case and 0.5% for the harsh focused wave.

Figure 12 presents a snapshot of the FOWT at the focus time ($t = 50$ s). We see that the FOWT is rather stable, the pitch angle is small and there is not much vorticity generated. The wave run-up on the central column has not reached the position of the braces, so the omission of the braces and tower in the simulation will not induce any significant errors.

Setting $t \in [30, 100]$ s, we find the computational times for the harsh focused wave case to be 21.1 and 25.3 k CPU hours for using no fluid-mooring coupling and the one-way fluid mooring coupling, respectively. We thus see a 20% computational overhead from the one-way coupling. This is arguably a high value, however, the implementation uses a simplistic cell-stepping algorithm to locate cells with individual mooring points. A significant speedup is expected when a more efficient cell-search algorithm is implemented.

CONCLUSIONS

A 1:70 scale model of the slack-moored UMaine VoltturnUS-S semi-submersible platform was modelled using the incompressible two-phase Navier-Stokes code in the OpenFoam framework coupled to the dynamic mooring solver moodyCore. As the mooring system was a bit undetermined in the experimental campaign, initially the mooring set-up was tested using measured locations of the fairleads. We saw that the numerical simulation using static fairleads did not give as large difference between fore and aft lines as the experiments. Both the decay as focused wave cases showed a good capture of the dynamics but with constant offsets – overall the tension in the fore line is under-predicted by the numerics.

The difference in mooring forces subsequently led to slightly different equilibrium position compared to the experiment. However, the differences are relatively minor, less than a centimeter in translation and 2/10:th of a degree in rotation.

The numerical decay tests showed a good overall agreement to the experiments. The surge amplitude was slightly over-predicted and the pitch period slightly too small, but generally a very satisfactory

comparison to the experiments was found.

Also the focused wave cases showed good overall agreement. The main reason for the discrepancy is likely due to difference in equilibrium position. Also the reduced length of the wave basin introduces a phase error for the preceding trough, as apparent from the empty wave tank tests.

Finally, while we saw that the mooring forces became larger using the fluid-mooring coupling, there was only very minor effect on the motion response of the FOWT. This is likely due to the rather short duration of the focused wave. For an embedded focused wave we expect the one-way coupling to give more accurate results. Unfortunately, the one-way coupling carries a significant computational overhead in its present form. The algorithm of finding the cell to sample for each mooring node is a computational bottleneck, and a significant speedup is expected when an improved method is implemented. This is ongoing work.

ACKNOWLEDGEMENTS

Support for this work was given by the Swedish Energy Agency through Grant No. 44423-2 and EU Horizon through the MSCA-PF Grant No. 101068736. Computations were performed on resources at (i) the National Supercomputer Centre provided by SNIC, partially funded by the Swedish Research Council through Grant Agreement No. 2018-05973; and (ii) LUMI through DeiC National HPC Grant Agreement No. DeiC-AAU-N3-2023017.

REFERENCES

Allen, C., A. Viscelli, H. Dagher, A. Goupee, E. Gaertner, N. Abbas, M. Hall, & G. Barter (2020). Definition of the UMaine VoltturnUS-S reference platform developed for the IEA wind 15-megawatt offshore reference wind turbine. <https://www.osti.gov/biblio/1660012>.

Burmester, S., G. Vaz, & O. el Moctar (2020). Towards credible CFD simulations for floating offshore wind turbines. *Ocean Engineering* 209, 107237.

Burmester, S., G. Vaz, O. el Moctar, S. Gueydon, A. Koop, Y. Wang, & H. Chen (2020). High-fidelity modelling of floating offshore wind turbine platforms. In *Proceedings of the 39th International Conference on Ocean, Offshore & Arctic Engineering*.

Cheng, P., Y. Huang, & D. Wan (2019). A numerical model for fully coupled aero-hydrodynamic analysis of floating offshore wind turbine. *Ocean Engineering* 173, 183–196.

de Lataillade, T. (2019). *High-Fidelity Computational Modelling of Fluid-Structure Interaction for Moored Floating Bodies*. Ph. D. thesis, University of Edinburgh.

DNV (2010). *Position Mooring*. Det Norske Veritas. Offshore standard DNV-OS-301.

Eskilsson, C. & J. Palm (2022). High-fidelity modelling of moored marine structures: multi-component simulations and fluid-mooring coupling. *Journal of Ocean Engineering and Marine Energy* 8(4), 513–526.

Jacobsen, N., D. Fuhrman, & J. Fredsoe (2012). A wave generation toolbox for the open-source CFD-library OpenFOAM. *Int. J. Num. Meth. Fluids* 70, 1073–1088.

Liu, Y., Q. Xiao, A. Incecik, C. Peyrard, & D. Wan (2017). Establishing a fully coupled CFD analysis tool for floating offshore wind turbines. *Renewable Energy* 112, 280–301.

Martin, T. & H. Bihs (2021). A numerical solution for modelling mooring dynamics, including bending and shearing effects, using a geometrically exact beam model. *J. Mar. Sci. Eng.* 9, 486.

Menter, F., M. Kuntz, & R. Langtry (2003). Ten years of industrial experience with the SST turbulence model. In *Proceedings of the fourth International Symposium on Turbulence, Heat and Mass Transfer*, Antalya, Turkey, pp. 625–632. Begell House.

OpenFast (2023). <https://github.com/openfast/openfast>.

OpenFOAM (2020). <http://www.openfoam.com>.

Palm, J. & C. Eskilsson (2018). *MOODY: User's manual version 2.0*. Available www.github.com/johannep/moodyAPI/releases.

Palm, J. & C. Eskilsson (2022). Facilitating large-amplitude motions of wave energy converters in OpenFOAM by a modified mesh morphing approach. *International Marine Energy Journal* 5(3), 257–264.

Palm, J., C. Eskilsson, & L. Bergdahl (2017). An *hp*-adaptive discontinuous Galerkin method for modelling snap loads in mooring cables. *Ocean Engineering* 144, 266–276.

Palm, J., C. Eskilsson, G. M. Paredes, & L. Bergdahl (2016). Coupled mooring analysis for floating wave energy converters using CFD: Formulation and validation. *Int. J. Mar. Energy* 16, 83–99.

Principia (2023). <http://www.principia-group.com/wp-content/uploads/2016/12/2-deelines-wind-presentation.pdf>.

Ransley, E., S. Brown, E. Edwards, T. Tosdevin, K. Monk, A. Reynolds, D. Greaves, & M. Hann (2022). Hydrodynamic response of a floating offshore wind turbine (1st fowt comparative study dataset). Pearl research repository <https://doi.org/10.24382/71j2-3385>.

Robertson, A., F. Wendt, J. Jonkman, W. Popko, H. Dagher, S. Gueydon, Q. J., F. Vittori, E. Uzunogulo, & R. Harries (2017). OC5 project phase II: Validation of global loads of the DeepCwind floating semisubmersible wind turbine. *Energy Procedia* 137, 38–57.

Shoemake, K. (1985). Animating rotation with quaternion curves. In *Special Interest Group on Computer Graphics and Interactive Techniques*, Volume 19. San Francisco, USA.

Tromans, P., A. Anaturk, & A. Hagemeijer (1991). A new model for the kinematics of large ocean waves-application as a design wave. In *Proceedings from the 1st International Offshore and Polar Engineering Conference (ISOPE)*, Edinburgh, UK, pp. 64–71.

Wang, L., A. Robertson, J. Jonkman, & Y. Yu (2021). Uncertainty assessment of CFD investigation of the nonlinear difference-frequency wave loads on a semisubmersible FOWT platform. *Sustainability* 13(64).

Weller, H., G. Tabor, H. Jasak, & C. Fureby (1998). A tensorial approach to computational continuum mechanics using object-oriented techniques. *Computers in Physics* 12(6), 620–631.

WFO (2020). Global offshore wind report 2019. Technical report, World Forum Offshore Wind.

Yu, Z., Q. Ma, X. Zheng, K. Liao, H. Sun, & A. Khayyer (2023). A hybrid numerical model for simulating aero-elastic-hydro-mooring-wake dynamic responses of floating offshore wind turbine. *Ocean Engineering* 268, 113050.

Zhou, Y., Q. Xiao, Y. Liu, A. Incecik, C. Peyrard, D. Wan, G. Pan, & S. Li (2022). Exploring inflow wind condition on floating offshore wind turbine aerodynamic characterisation and platform motion prediction using blade resolved CFD simulation. *Renewable Energy* 182, 1060–1079.